Spatial-temporal control of interferences of multiple tunneling photoelectron wave packets

Min Li,[1,2] Ji-Wei Geng,[1] Ming-Ming Liu,[1] Xu Zheng,[1] Liang-You Peng,[1,3,*] Qihuang Gong,[1,3] and Yunquan Liu[1,3,†]

[1]*Department of Physics and State Key Laboratory for Mesoscopic Physics, Peking University, Beijing 100871, People's Republic of China*

[2]*Wuhan National Laboratory for Optoelectronics and School of Physics, Huazhong University of Science and Technology, Wuhan 430074, People's Republic of China*

[3]*Collaborative Innovation Center of Quantum Matter, Beijing 100871, People's Republic of China*

(Received 9 February 2015; published 21 July 2015)

We theoretically study the control of the interferences of multiple tunneling photoelectron wave packets in both temporal and spatial domains by an orthogonally polarized two-color laser pulse. Profound carpetlike and stripelike interference patterns can be turned on or off in the momentum spectra using a weak streaking field at half the frequency of a strong fundamental field. The modulations of the interference patterns with respect to the relative phase between the two frequency components are well recaptured by both a semiclassical interference model and an *ab initio* simulation with numerically solving the time-dependent Schrödinger equation. We highlight the importance of the ionic Coulomb potential on the photoelectron angular distributions of atoms in the orthogonally polarized two-color pulses. It is shown that the interference induced by the forward rescattering trajectories is enhanced while the contribution of the direct trajectories is suppressed. This study offers alternative routes toward probing and controlling the ultrafast ionization dynamics of atoms and molecules.

DOI: 10.1103/PhysRevA.92.013416 PACS number(s): 32.80.Rm, 31.90.+s, 32.80.Fb, 32.80.Wr

The tunneling of an electron wave packet from the suppressed atomic potential is a fundamental process when atoms are subjected to a strong laser field [1]. For a long laser pulse, a sequence of electron wave packets will be emitted near the field maxima. The electron wave packets initiated by the tunneling are confined to subfemtosecond intervals, laying the foundation for the prosperous attosecond physics [2]. Generally, the wave packets following different pathways from a specified initial state to the same final state will give rise to the quantum interference effect. The interference patterns of these tunneled wave packets usually encode high-resolution spatial and temporal information of the nucleus and the photoelectron [3], which can be used to extract the phase information of electronic wave packets in momentum space [4] and to characterize the alignment-dependent spatial phase of the tunneling wave packet in molecules [5]. Precise manipulation of the wave-packet interference is the primary step toward developing interferometric technology to probe ultrafast multielectron dynamics [6] and to control chemical reaction.

Usually, the wave packets tunneled at each field maximum are not separated. One of the most fundamental interference effects among those wave packets is the periodic peak structure in the electron energy spectrum, i.e., the above-threshold ionization (ATI) peak [7], which arises from the intercycle interference of electron wave packets released at time intervals separated by a laser cycle [8]. Recently, subcycle photoelectron interference has attracted more attention and it has been comprehensively studied in a single-color laser field, such as the time-domain double-slit interference [9–12], and the recollision-induced photoelectron holographic interference [3,13–15]. The formation of photoelectron angular distributions (PADs) in ATI has been revealed in terms of the interference of trajectories [16]. By adding a second harmonic field parallel to the fundamental field, the electron emission time and the subcycle interference can be controlled on an attosecond time scale [17]. Making use of orthogonally polarized two-color (OTC) laser fields allows one to resolve and control the ultrafast electron dynamics in two-dimensional space in single ionization [18–20], nonsequential double ionization [21], and high-harmonic generation [22,23].

In the present work, we study the photoelectron angular distributions of atoms in an OTC pulse consisting of 800-nm (ionization) and 1600-nm (streaking) laser fields. Profound interference patterns beyond the above-threshold ionization, i.e., carpetlike and stripelike structures, can be revealed by a semiclassical simulation and by a numerical solution of the time-dependent Schrödinger equation (TDSE). Using the weak streaking field at long wavelength, we show that multiple tunneling wave packets can be spatially and temporally controlled by tuning the relative phase between the two frequency components. Through controlling electron bursts within each laser cycle, we disentangle the contributions of the subcycle interference at different time scales. We further show that the long-range Coulomb potential has a dominant role on the momentum spectra, which will enhance the interference induced by the forward rescattering trajectories and suppress the interference by the direct trajectories.

We first use a semiclassical interference model to study the interference of multiple wave packets in OTC laser fields [16]. Briefly, we prepare the tunneling wave packet using Monte Carlo methods, in which the electron is released at an initial position (tunnel exit) derived from Landau's effective potential theory [24] with zero initial longitudinal momentum along the instantaneous laser field direction. The time-dependent tunneling ionization rate and the initial momentum distribution transverse to the instantaneous laser field direction are given by the Ammosov-Delone-Krainov theory [25]. The OTC laser field is given by $\mathbf{E}(t) = E_0 f(t)\cos(\omega t)\mathbf{z} + aE_0 f(t)\cos[\frac{1}{2}(\omega t + \Delta\varphi)]\mathbf{x}$, where $f(t)$ is the pulse envelope, and E_0 and ω are the amplitude and frequency of the 800-nm fundamental laser field, respectively. Atomic units are used

*liangyou.peng@pku.edu.cn
†yunquan.liu@pku.edu.cn

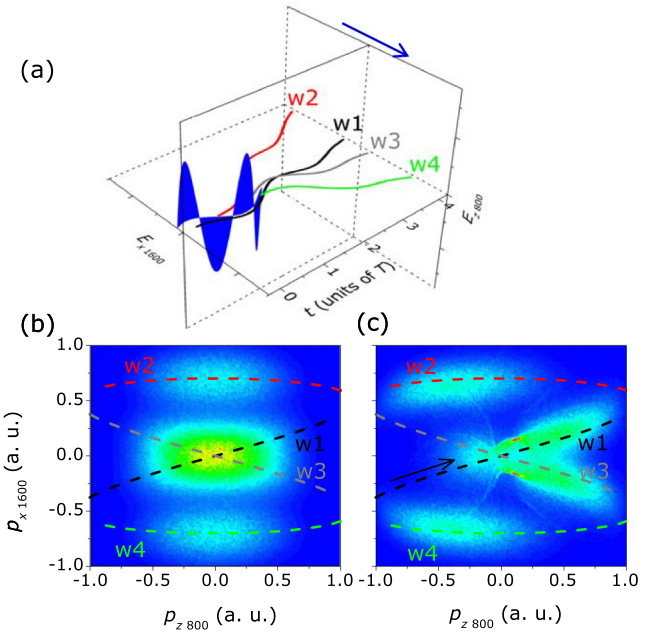

FIG. 1. (Color online) (a) Separating multiple tunneling wave packets that are produced by a strong 800-nm field using a weak streaking field at 1600 nm. Each cycle of the OTC pulse (blue area) launches four electron wave packets (black for w1, red for w2, gray for w3, and green for w4) through the tunneling near the field maximum. The weak 1600-nm streaking field steers the electron motion in the lateral direction (indicated by the blue arrow), as shown by the trajectories of the four wave packets. Also shown are the simulated photoelectron angular distributions by the semiclassical model (b) without and (c) with the Coulomb potential. Here the interference effect is ignored. The field-driven photoelectron momenta $\mathbf{p} = -\mathbf{A}(t_0)$ of the four wave packets are shown by the dashed curves with different colors. The arrow in (c) shows the time evolution direction. The laser intensity is 1.4×10^{14}W/cm^2 for 800 nm and 1.4×10^{13}W/cm^2 for 1600 nm and $\Delta\varphi = 0$.

throughout unless otherwise specified. Here a and $\Delta\varphi$ are the ratio of field strength and the relative phase of the two frequency components.

We use a weak 1600-nm field ($a = 1/\sqrt{10}$) to steer the electron wave packets ionized by a strong 800-nm fundamental field. The laser field is chosen such that the weak streaking field plays a minor role in the tunneling process but can effectively streak the wave packet in the subsequent propagation process due to the long wavelength. In such a pulse, a wave packet is tunneled in each half cycle of the 800-nm field. Hence, there will be four wave packets for each period of the OTC field $T' = 2T$ (T is the period of the 800-nm field), which are labeled as w1, w2, w3, and w4 in Fig. 1(a). After tunneling, the evolution of those wave packets in the combined oscillating laser field and Coulomb field is solved via the Newtonian equation $\ddot{\mathbf{r}} = -\mathbf{r}/r^3 - \mathbf{E}(t)$ (r is the distance between the electron and the nucleus). At the same time, each trajectory will acquire a phase accumulated along the path [26] $S = \int_{t_0}^{\infty} [\mathbf{v}^2(t)/2 - 1/r + I_p]dt$, where t_0 is the electron ionization time, $\mathbf{v}(t)$ is the electron velocity, and I_p is the ionization potential. The final photoelectron momentum spectrum is the coherent superposition of all the trajectories. In the simulation, the laser envelope is trapezoidal with a two-cycle turn-on, a four-cycle plateau, and a two-cycle turn-off for the 800-nm field. We have restricted the electrons to motion in the z-x polarization plane with $y = 0$ for simplicity.

Depending on the vector potential at the instant of ionization, the tunneled wave packet will obtain a lateral momentum of almost $p_x = -A_x(t_0) = 2aE_0/\omega \sin[\frac{1}{2}(\omega t_0 + \Delta\varphi)]$, as shown by the typical trajectories for the four wave packets in Fig. 1(a) for $\Delta\varphi = 0$. Therefore, the streaking field can separate two wave packets along the x direction by up to $4aE_0/\omega$. The transverse momentum width for each wave packet with the Gaussian distribution after the tunneling is given by $\sigma_\perp = (E_0/\sqrt{2I_p})^{1/2}$ [25]. To separate the wave packets by $2\sigma_\perp$ [27], the ratio of the field strength between the streaking field and the fundamental field is required to satisfy $a > \frac{1}{2}\omega {E_0}^{-1/2}(2I_p)^{-1/4} = 0.11$. Using the long-wavelength light as the streaking field, a small field strength is sufficient to spatially control the separation and overlap of the wave packets.

Because the electrons ionized at different t_0 will be streaked to different final momenta, we further study the final momentum distributions of the four wave packets. If the Coulomb effect is not included, the calculated momentum distributions without both the Coulomb potential and the trajectory phase are illustrated in Fig. 1(b) when $\Delta\varphi = 0$. The final momentum can be estimated by the field-driven momentum $\mathbf{p} = -\mathbf{A}(t_0)$ for the four wave packets by the dashed curves in Fig. 1(b). The four wave packets are parallel to each other along the horizonal direction in the momentum spectrum. The final momenta of the wave packets of w1 and w3 were around zero and would overlap with each other. If the Coulomb potential is included, the simulated momentum distribution is shown in Fig. 1(c). It is clearly seen that the central position of each wave packet is shifted with respect to the axis of $p_z = 0$ by an offset angle, which is similar to the case of Coulomb asymmetry in elliptically polarized laser fields [27,28]. Compared to Fig. 1(b), the direction of the angular shift of each wave packet depends on the ionization time, e.g., the wave packets of w1 and w3 tilt to the positive p_z direction while the wave packets of w2 and w4 tilt to the negative p_z direction. The momentum distributions of the wave packets of w1 and w3 are separated at $\Delta\varphi = 0$. Due to the Coulomb effect, the momentum distributions of the electron wave packets in the p_z direction can also be controlled by the weak streaking field.

To reveal the controlled interference of multiple tunneling wave packets, we show the simulated two-dimensional PADs with respect to the relative phase without and with the Coulomb effect by the semiclassical interference model in Figs. 2(a) and 2(b), respectively. One can clearly observe that all the momentum distributions will be strongly distorted because of the Coulomb effect, revealing spatially asymmetric distributions.

To validate the simulated results by the semiclassical interference model, we have performed a three-dimensional *ab initio* TDSE calculation for a hydrogen atom with the Coulomb potential. In Fig. 2(c) we present the PADs in the polarization plane for different phases by the TDSE calculations with the same laser parameter as the semiclassical calculation. The PADs are obtained by projecting the wave function onto

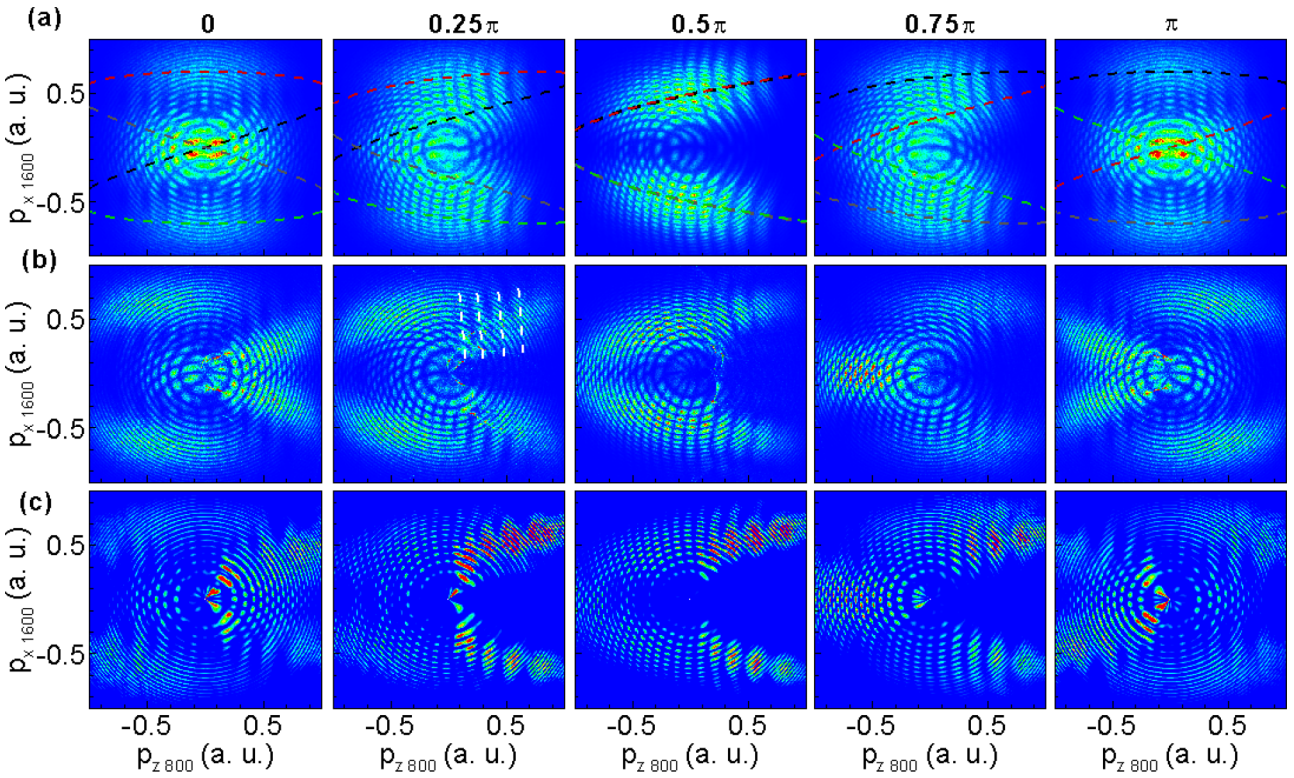

FIG. 2. (Color online) The simulated two-dimensional PADs of a hydrogen atom (a) without and (b) with the Coulomb potential by the semiclassical interference model. The bottom panel (c) shows the *ab initio* TDSE results. The relative phase of the OTC field is labeled at the top of the figure. The field-driven photoelectron momenta $\mathbf{p} = -\mathbf{A}(t_0)$ of the four wave packets are shown in (a) by the dashed curves with different colors (black for w1, red for w2, gray for w3, and green for w4). The white dashed lines in (b) show the stripelike interference patterns. The laser intensity is $1.4 \times 10^{14}\mathrm{W/cm^2}$ for 800 nm and $1.4 \times 10^{13}\mathrm{W/cm^2}$ for 1600 nm.

the Coulomb continuum scattering eigenstates after the time-dependent propagation using a grid-based split-step method [29]. The momentum distributions of the TDSE calculation show the same spatial asymmetry as the semiclassical results. The good agreement between the TDSE and the semiclassical results demonstrates the importance of the Coulomb potential in the formation of the PADs. The observed features in the pure quantum calculation are well recaptured by the semiclassical interference model.

Both the TDSE and the semiclassical simulations reveal many interference patterns. First, all the spectra display ring-like interference patterns centered around zero momentum, which arise from the intercycle interference. Those intercycle interference rings are nearly independent of the relative phase.

Second, there are other abundant interference patterns in the momentum spectrum. These features come from the subcycle interference among the wave packets and they vary differently as a function of the relative phase of the OTC fields. One of the clear subcycle interference patterns is the stripelike structure along the p_x direction [14], as shown by the white dashed lines in Fig. 2(b) at $\Delta\varphi = 0.25\pi$. In the Coulomb-free case [Fig. 2(a)], this stripelike structure can be obviously seen in all the phases of the OTC fields. With considering the Coulomb potential, the stripelike structure appears when $p_z > 0$ at the phase of 0.25π, 0.5π, and 0.75π, and it is nearly turned off at $\Delta\varphi = 0$ and $\Delta\varphi = \pi$. Moreover, there is another interference pattern in the p_z direction. This interference pattern manifests itself as the absence of every other ATI peak when $p_x = 0$. This carpetlike interference pattern is observed in the transverse direction with respect to the field polarization in a single-color pulse [12], but here it appears in the longitudinal direction of the fundamental field (p_z direction). This carpetlike pattern is highly enhanced at $\Delta\varphi = 0.75\pi$ and is suppressed at $\Delta\varphi = 0.25\pi$ when considering the Coulomb potential.

All the interference patterns by the semiclassical interference model [Fig. 2(b)] can be well reproduced by the TDSE calculation [Fig. 2(c)], including the stripelike and carpetlike structures. The modulations of these interference structures with respect to $\Delta\varphi$ are quite similar. Taking advantage of the semiclassical interference model, we can decouple the contributions of the subcycle interference on the spatially asymmetric momentum distributions. Figure 3 shows different subcycle interferences at $\Delta\varphi = 0.25\pi$ and $\Delta\varphi = 0.75\pi$. The interference of w1 and w2 leads to the stripelike pattern for both $\Delta\varphi = 0.25\pi$ and $\Delta\varphi = 0.75\pi$. In contrast, the carpetlike structure arises from the interference of w1 with w3 for $\Delta\varphi = 0.25\pi$ and from the interference of w2 with w4 for $\Delta\varphi = 0.75\pi$. The carpetlike structure can be explained within a simple picture: In each cycle of the OTC field, there are two ionization times at which the vector potential of the streaking field is zero. These two ionization times are separated by a half cycle of the OTC field, corresponding to the subcycle interferences of w1 with w3 or w2 with w4. The stripelike and carpetlike interference patterns correspond to the subcycle interference at different time scales, thus leading to different interference fringes in the momentum spectrum.

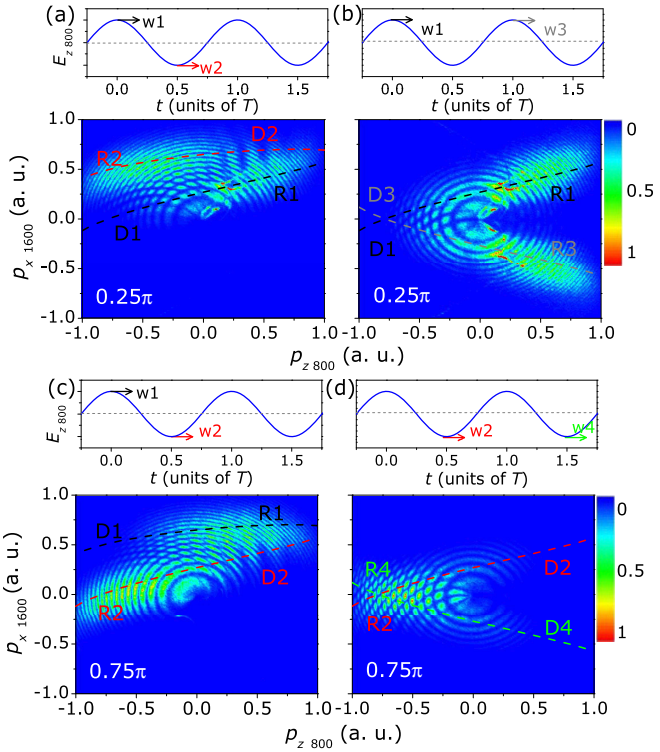

FIG. 3. (Color online) Subcycle interference of the wave packets at different time scales in the OTC field of $\Delta\varphi = 0.25\pi$ [(a) and (b)] and $\Delta\varphi = 0.75\pi$ [(c) and (d)]. The top panels of each plot show the 800-nm electric field of the OTC pulse. The bottom panels show the semiclassical simulation that includes the selected wave packets in each cycle of the OTC pulse. The dashed curves show the field-driven photoelectron momenta $\mathbf{p} = -\mathbf{A}(t_0)$. See text for the definition of the direct trajectory Dn and rescattering trajectory Rn for the four wave packets. The laser intensity is $1.4 \times 10^{14}\mathrm{W/cm^2}$ for 800 nm and $1.4 \times 10^{13}\mathrm{W/cm^2}$ for 1600 nm.

In Fig. 3, the dashed curves show the field-driven momentum $\mathbf{p} = -\mathbf{A}(t_0)$ of each wave packet. One should note that in the Coulomb-free case, the PADs would be the same for 0.25π and 0.75π because of the same field vector potential, as shown in Fig. 2(a). It is very interesting that the photoelectron momentum distributions are strikingly different at those two relative phases as seen in Figs. 3(a) and 3(c) or Figs. 3(b) and 3(d). This difference indicates that the Coulomb potential plays an essential role in the formation of the PADs of the interference from multiple photoelectron wave packets.

To shed light on the formation of the spatially asymmetric momentum distributions, we need to further study the sub-half-cycle dynamics of the photoelectrons in the OTC fields. According to the model first proposed by van Linden van den Heuvell and Muller [30], which neglects the long-range Coulomb effect on the classical trajectories, there will be two groups of trajectories for an ionization burst in each half cycle: (i) the electron emitted prior to the field maximum at a quarter cycle of the 800-nm field is directly pulled away from the nucleus, which is referred to as direct trajectories; and (ii) the electron ionized after the field maximum will be scattered by the nucleus, which is referred to as rescattering trajectories. Due to the streaking field, the rescattering electrons will miss the direct impaction on the nucleus and will be scattered forward. A more detailed description of the direct and rescattering trajectories can be found in the supplementary material of Ref. [28]. Depending on the ionization time, the direct and rescattering trajectories for the four wave packets are shown by Dn and Rn ($n = 1$, 2, 3, 4 for w1, w2, w3, and w4) in Fig. 3, respectively. One can clearly find that, in each electron wave packet, the relative contribution of the direct trajectories is suppressed and the relative yields of the forward scattering trajectories are increased in the presence of the Coulomb potential. Due to the Coulomb attraction, more electrons can be driven back and be scattered by the nucleus. As a result, the angular offset of each wave packet tilts toward the forward scattering trajectories. In Figs. 3(a) and 3(c), the stripelike pattern looks similar at the phases of 0.25π and 0.75π because it arises from the subcycle interference among the direct trajectories of w2 (D2) and the forward rescattering trajectories of w1 (R1). This stripelike interference will be enhanced at $\Delta\varphi = 0.5\pi$ due to the maximum overlap of D2 and R1 wave packets and it will become hard to distinguish when the two wave packets are almost completely separated at $\Delta\varphi = 0$ and $\Delta\varphi = \pi$, as seen in Fig. 2. The carpetlike structure comes from the interference of the direct trajectories of D1 and D3 at $\Delta\varphi = 0.25\pi$ while from the interference of the forward rescattering trajectories of R2 and R4 at $\Delta\varphi = 0.75\pi$. The interference among the forward scattering trajectories is highly enhanced at the phase of 0.75π [Fig. 3(d)] and the interference induced by direct trajectories is suppressed at the phase of 0.25π [Fig. 3(b)]. As a result, the final PADs reveal prominent differences although the field vector potentials are the same.

In conclusion, we have studied the spatial and temporal manipulation of the interferences of multiple tunneling wave packets using a weak streaking field at a long wavelength. Profound interference patterns, i.e., stripelike and carpetlike in the momentum spectra can be turned on or off by tuning the relative phase of the OTC fields. These structures originate from the subcycle interference at different time scales. Their contributions to the photoelectron angular distributions are disentangled within each laser cycle in the semiclassical interference model. We further show that, due to the effect of the long-range Coulomb potential, the interference by the forward rescattering trajectories is enhanced while that by the direct trajectories is suppressed.

The interference pattern has encoded the initial phase information of the tunneling current when applied to molecules [5]. In molecules, the initial phase of the tunneling wave packet is much more complex than that of atoms. Using our two-color control scheme, the modulation of the interferogram in both temporal and spatial domains might pave the way to extracting this initial phase of molecules, which could lead to the complete characterization, both amplitude and phase, of the molecular tunneling wave packet. The modulation of the interference patterns also has significant implications in time-resolving electron dynamics in atoms and molecules [4,17]. For instance, the relative spectral phase of adjacent ATI channels depends sensitively on the laser fields. By changing the relative phase of a two-color field, the interfering ionization signal can be used to probe the phase delays of the ATI spectrum [18].

This work is supported by the National Program on Key Basic Research Project (2013CB922402 and 2013CB922403), the NSFC (No.11434002, No.11134001, and No.11322437) and the NCET in University from Ministry of Education. Y.L. acknowledges support by the National Science Fund for Distinguished Young Scholars in China (No. 11125416).

[1] L. V. Keldysh, Zh. Eksp. Teor. Fiz. **47**, 1945 (1964) [Sov. Phys. JETP **20**, 1307 (1965)].
[2] F. Krausz and M. Ivanov, Rev. Mod. Phys. **81**, 163 (2009).
[3] Y. Huismans *et al.*, Science **331**, 61 (2011); Phys. Rev. Lett. **109**, 013002 (2012).
[4] T. Remetter *et al.*, Nat. Phys. **2**, 323 (2006).
[5] M. Meckel, A. Staudte, S. Patchkovskii, D. M. Villeneuve, P. B. Corkum, R. Dörner, and M. Spanner, Nat. Phys. **10**, 594 (2014).
[6] O. Smirnova, Y. Mairesse, S. Patchkovskii, N. Dudovich, D. Villeneuve, P. Corkum, and M. Yu. Ivanov, Nature (London) **460**, 972 (2009).
[7] P. Agostini, F. Fabre, G. Mainfray, G. Petite, and N. K. Rahman, Phys. Rev. Lett. **42**, 1127 (1979).
[8] D. G. Arbó, K. L. Ishikawa, K. Schiessl, E. Persson, and J. Burgdörfer, Phys. Rev. A **81**, 021403(R) (2010).
[9] F. Lindner, M. G. Schatzel, H. Walther, A. Baltuska, E. Goulielmakis, F. Krausz, D. B. Milosevic, D. Bauer, W. Becker, and G. G. Paulus, Phys. Rev. Lett. **95**, 040401 (2005).
[10] D. G. Arbó, E. Persson, and J. Burgdörfer, Phys. Rev. A **74**, 063407 (2006).
[11] R. Gopal *et al.*, Phys. Rev. Lett. **103**, 053001 (2009).
[12] P. A. Korneev *et al.*, Phys. Rev. Lett. **108**, 223601 (2012).
[13] D. Hickstein *et al.*, Phys. Rev. Lett. **109**, 073004 (2012).
[14] X.-B. Bian, Y. Huismans, O. Smirnova, K.-J. Yuan, M. J. J. Vrakking, and A. D. Bandrauk, Phys. Rev. A **84**, 043420 (2011).
[15] X. B. Bian and A. D. Bandrauk, Phys. Rev. Lett. **108**, 263003 (2012); M. Li *et al.*, Sci. Rep. **5**, 8519 (2015).
[16] M. Li, J.-W. Geng, H. Liu, Y. Deng, C. Wu, L. Y. Peng, Q. Gong, and Y. Liu, Phys. Rev. Lett. **112**, 113002 (2014).
[17] X. Xie *et al.*, Phys. Rev. Lett. **108**, 193004 (2012); D. G. Arbó, S. Nagele, X. M. Tong, X. Xie, M. Kitzler, and J. Burgdörfer, Phys. Rev. A **89**, 043414 (2014).
[18] L. J. Zipp, A. Natan, and P. H. Bucksbaum, Optica **1**, 361 (2014).
[19] L. Zhang *et al.*, Phys. Rev. A **90**, 061401(R) (2014).
[20] M. Richter, M. Kunitski, M. Schoffler, T. Jahnke, L. P. H. Schmidt, M. Li, Y. Liu, and R. Dörner, Phy. Rev. Lett. **114**, 143001 (2015).
[21] L. Zhang *et al.*, Phys. Rev. Lett. **112**, 193002 (2014).
[22] M. Kitzler and M. Lezius, Phys. Rev. Lett. **95**, 253001 (2005).
[23] D. Shafir, H. Soifer, B. D. Bruner, M. Dagan, Y. Mairesse, S. Patchkovskii, M. Yu. Ivanov, O. Smirnova, and N. Dudovich, Nature (London) **485**, 343 (2012).
[24] L. D. Laudau and E. M. Lifshitz, *Quantum Mechanics* (Pergamon, Oxford, 1977).
[25] M. V. Ammosov, N. B. Delone, and V. P. Krainov, Zh. Eksp. Teor. Fiz. **91**, 2008 (1986) [Sov. Phys. JETP **64**, 1191 (1986)]; N. B. Delone and V. P. Krainov, J. Opt. Soc. Am. B **8**, 1207 (1991).
[26] G. G. Paulus, F. Linder, D. B. Milošević, and W. Becker, Phys. Scr. T **110**, 120 (2004).
[27] D. Shafir, H. Soifer, C. Vozzi, A. S. Johnson, A. Hartung, Z. Dube, D. M. Villeneuve, P. B. Corkum, N. Dudovich, and A. Staudte, Phys. Rev. Lett. **111**, 023005 (2013).
[28] M. Li, Y. Liu, H. Liu, Q. Ning, L. Fu, J. Liu, Y. Deng, C. Wu, L.-Y. Peng, and Q. Gong, Phys. Rev. Lett. **111**, 023006 (2013).
[29] L. Peng, E. Pronin, and A. Starace, New J. Phys. **10**, 025030 (2008).
[30] H. B. van Linden van den Heuvell and H. G. Muller, in *Multiphoton Processes*, edited by S. J. Smith and P. L. Knight (Cambridge University, New York, 1988).